Title
An assessment of ozone photochemistry in the extratropical western North Pacific: Impact of continental outflow during the late winter/early spring

Journal
Journal of Geophysical Research Atmospheres, 102(23)

ISSN
0148-0227

Authors
Crawford, J
Davis, D
Chen, G
et al.

Publication Date
1997-12-20

DOI
10.1029/97jd02600

JOURNAL OF GEOPHYSICAL RESEARCH, VOL. 102, NO. D23, PAGES 28,469-28,487, DECEMBER 20, 1997

An assessment of ozone photochemistry in the extratropical western North Pacific: Impact of continental outflow during the late winter/early spring

J. Crawford,[1,3] D. Davis,[1] G. Chen,[1] J. Bradshaw,[1] S. Sandholm,[1] Y. Kondo,[2] S. Liu,[1] E. Browell,[3] G. Gregory,[3] B. Anderson,[3] G. Sachse,[3] J. Collins,[4] J. Barrick,[3] D. Blake,[5] R. Talbot,[6] and H. Singh[7]

Abstract. This study examines the influence of photochemical processes on tropospheric ozone distributions over the extratropical western North Pacific. The analysis presented here is based on data collected during the Pacific Exploratory Mission-West Phase B (PEM-West B) field study conducted in February-March 1994. Sampling in the study region involved altitudes of 0-12 km and latitudes of 10°S to 50°N. The extratropical component of the data set (i.e., 20-50°N) was defined by markedly different photochemical environments north and south of 30°N. This separation was clearly defined by an abrupt decrease in the tropopause height near 30°N and a concomitant increase in total O_3 column density. This shift in overhead O_3 led to highly reduced rates of O_3 formation and destruction for the 30-50°N latitude regime. Both latitude ranges, however, still exhibited net O_3 production at all altitudes. Of special significance was the finding that net O_3 production prevailed even at boundary layer and lower free tropospheric altitudes (e.g., $\leq$ 4 km), a condition uncommon to Pacific marine environments. These results reflect the strong impact of continental outflow of O_3 precursors (e.g., NO and NMHCs) into the northwestern Pacific Basin. Comparisons with PEM-West A, which sampled the same region in a different season (September-October), revealed major differences at altitudes below 4 km, the altitude range most influenced by continental outflow. The resulting net rate of increase in the tropospheric O_3 column for PEM-West B was 1-3% per day, while for PEM-West A it was approximately zero. Unique to the PEM-West B study is the finding that even under wintertime conditions substantial column production of tropospheric O_3 can occur at subtropical and mid-latitudes. While such impacts may not be totally unexpected at near coast locations, the present study suggests that the impact from continental outflow on the marine BL could extend out to distances of more than 2000 km from the Asian Pacific Rim.

1. Introduction

The importance of O_3 in tropospheric photochemistry is well established. It is central to determining the oxidative capacity of the atmosphere. The photolysis of this species ($\lambda \leq 320$ nm) initiates the formation of the OH radical, and it is the follow-on free radical chemistry that is responsible for the removal of atmospheric pollutants. This free radical chemistry also contains feedbacks that can both produce as well as further destroy O_3 [e.g., *Chameides and Walker*, 1973; *Crutzen*, 1973; *Liu et al.*, 1980]. Depending on the environment, the combined effect of these feedbacks can result in either a net photochemical loss or gain of ozone. In studies of the global budget of tropospheric O_3, an issue of continuing interest has been determining the importance of photochemical sources and sinks relative to transport of O_3 from the stratosphere and surface loss [e.g., *Fabian*, 1974; *Chatfield and Harrison*, 1976; *Fabian and Pruchniewicz*, 1977; *Fishman et al.*, 1979; *Liu et al.*, 1980; *Gidel and Shapiro*, 1980; *Mahlman et al.*, 1980; *Chameides and Tan*, 1981; *Logan et al.*, 1981; *Logan*, 1985; *Isaksen and Hov*, 1987; *Hough and Derwent*, 1990; *Hough*, 1991; *Davis et al.*, 1996; *Jacob et al.*, 1996; *Thompson et al.*, 1996; *Crawford et al.*, this issue].

[1]School of Earth and Atmospheric Sciences, Georgia Institute of Technology, Atlanta.
[2]Solar Terrestrial Environmental Laboratory, Nagoya University, Toyokawa, Aichi, Japan
[3]NASA Langley Research Center, Hampton, Virginia.
[4]Science and Technology Corporation, Hampton, Virginia.
[5]Chemistry Department, University of California-Irvine.
[6]Institute for the Study of Earth, Oceans, and Space, University of New Hampshire, Durham.
[7]NASA Ames Research Center, Moffet Field, California.

Paper number 97JD02600.
0148-0227/97/97JD-02600$09.00

In an effort to expand the observational data base for evaluating the tropospheric O_3 budget, aircraft campaigns such as those sponsored by NASA's Global Tropospheric Experiment (GTE) have become centrally important. The Pacific Exploratory Mission in the western North Pacific (PEM-West) represents one of the most recent missions. It was conducted in two phases [*Hoell et al.*, 1996, this issue]. In the fall of 1991, PEM-West Phase A (PEM-A) sampled the western Pacific during a period when the mean flow was toward the Asian continent. Thus, it afforded an opportunity to observe this region under minimal anthropogenic influence. By contrast, PEM-West Phase B (PEM-B) was conducted during the winter of 1994 and sampled at a time during which there was maximum continental outflow. This outflow was mainly confined to extratropical latitudes (i.e., >20°N) although on occasion it penetrated as far south as 13°N [*Crawford et al.*, this issue; *Merrill et al.*, this issue].

In a companion paper we discuss the tropical component of PEM-B [*Crawford et al.*, this issue]. This paper will focus on the extratropical latitudes. Specific objectives will include (1) to assess the relative importance of the ozone-controlling chemical factors such as NO, NMHCs, H_2O, and peroxy radicals, (2) to assess the impact of photochemistry on the regional ozone budget, and (3) to evaluate seasonal differences in the photochemistry of the extratropical western Pacific through comparison with the first phase program, PEM-A.

2. Observational Database

2.1. Measurements

The basic suite of chemical species and physical variables measured during PEM-B was essentially unchanged from PEM-A [*Hoell et al.*, 1996]. Parameters specifically used to constrain the model calculations for this analysis are listed in Table 1. Specific details on individual measurement techniques as well as changes/improvements to previously employed instrumentation are given by *Hoell et al.* [this issue].

As in PEM-A, NO was measured using two independent techniques. The first group, from Georgia Institute of Technology, used a laser detection technique labeled by these investigators as "two-photon laser-induced fluorescence" (TP-LIF). The second group, associated with Nagoya University, employed the more common method of O_3 chemiluminescence. The results from these two approaches compared quite well for all PEM-B flights. A standard regression analysis of approximately 5000 paired NO measurements (30 s sample integration) gave a slope of 1.25 ± 0.01, an intercept of 1.2 ± 0.2 pptv, and an R^2 value of 0.95. On average, the Nagoya University NO data were found to be higher than those measured by Georgia Tech. Although this comparison only involved data with mixing ratios in the range of 0-200 pptv, these data constituted nearly 99% of the total data set. Given this good agreement, the modeling analysis presented here used NO values reported by both groups. For time periods where both groups reported NO values, the average was taken.

The analysis described in this work has been based on time-dependent box model calculations. These calculations have used median chemical and physical conditions for specific altitude/latitude sampling bins. A merged data set based on 30 s sampling time intervals was used to establish these median values. Before estimating these median values, however, the data set was filtered so as to include only data for solar zenith angles less than 60°. This restriction was imposed in an effort to deal with the fact that NO_2 measurements were not available. Since the partitioning of NO_x ($NO+NO_2$) changes rapidly during early morning and late afternoon, the exclusion of high zenith angle data tended to ensure that median NO values could be used with high confidence to infer values for median NO_x. Finally, data were filtered to include only data points for which valid measurements of all critical constituents (e.g., NO, O_3, CO, and H_2O) were present. Concerning NMHCs, concurrent measurements were available for only 37% of the data. For most of the remaining time periods, NMHC values were interpolated from measurements that bracketed the empty data slot (typically 4 min. or less). In these cases the continuity in O_3 and CO as well as NMHC levels themselves were used as criteria to determine whether the interpolation was reasonable. In cases where interpolation could not be justified (16%), median NMHC values for the appropriate altitude/latitude bin were used.

2.2 Geographic Distribution of Critical Species

Figure 1 shows the geographic distribution of samples taken during PEM-B. Symbols indicate the location of the more than 6800 observations (i.e., 30 s time intervals). For this analysis, these observations were assigned to one of three analysis regimes. The first division involved a separation of the data into tropical and extratropical regimes based on meteorological data which showed significant continental outflow (via frontal passage) into marine areas north of 20°N [*Merrill et al.*, this issue]. The extratropical region, north of 20°N, was then further separated into two subregimes encompassing the latitude ranges of 20-30°N and 30-50°N. The latter separation reflects the abrupt change observed in both the tropopause height and total O_3 column density. Plate 1 depicts the latitude-altitude distribution of O_3 as derived from the PEM-B UV-DIAL data and clearly shows the abrupt drop in tropopause height from ~16 km to 8-9 km near 30°N.

Table 1. Parameters Used to Constrain The Model

Chemical	O_3, CO, NO, C_2H_6, C_3H_8, ≥C_4 alkanes, C_2H_4, ≥C_3 alkenes, C_6H_6, aromatics, acetone, methanol, ethanol, formic acid, acetic acid, HNO_3, PAN
Physical	latitude, longitude, altitude, temperature, pressure, dew point, O_3 column density (Meteor-3 TOMS, version 7)

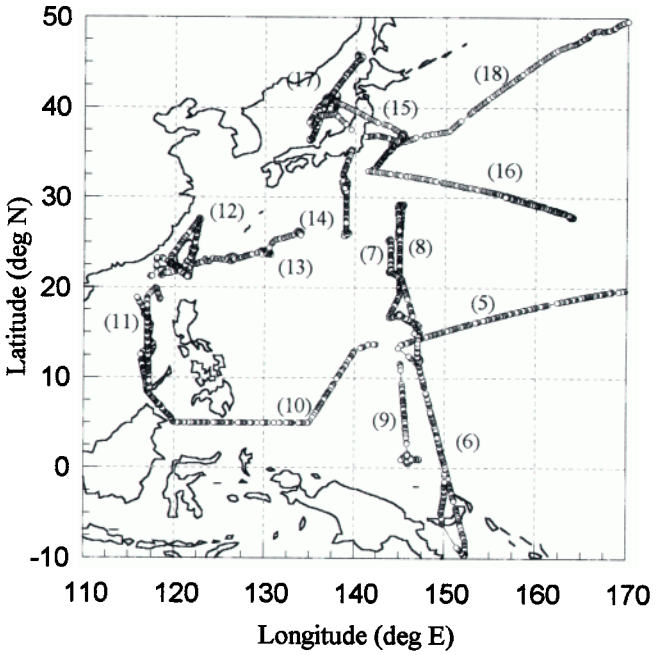

Figure 1. PEM-West B data collection region. Flight numbers are shown in parentheses. Circular symbols indicate individual in situ observations.

Also associated with this change was an increase in the median total O_3 column density of ~150 D.U. based on Meteor-3 TOMS data (Version 7).

Still other information justifying the proposed separation into two latitude regimes can be found in the latitude trends of several chemical species. For example, Figures 2a-2f show distributions of O_3, CO, NO, dew point, C_2H_6, and C_3H_8 for altitude ranges of 0-4, 4-8, and 8-12 km. As seen from Figure 2a, O_3 levels decrease southward from 20°N at all altitudes. However, north of 20°N there is no discernable gradient below 8 km. The increase in O_3 between 20 and 30°N for altitudes of 8-12 km most likely reflects the increasing influence of stratospheric intrusions. North of 30°N at 8-12 km, O_3 values less than 100 ppbv were observed mostly between 8-9 km. Quite consistent with the remote UV-DIAL data, two-thirds of the in situ O_3 data above 9 km ranged from 100-600 ppbv and are not seen in Figure 2a. As shown in Figure 2b, CO exhibits a rather abrupt change in its mixing ratio in the vicinity of 20°N, most likely reflecting the influence of continental outflow. Below 8 km, the highest values occur in the 20-30°N range; whereas, above 8 km, extreme values of CO are observed north of 30°N. The latter values were primarily recorded between 8-9 km during flight 16 which was intended to sample continental outflow behind a recent frontal passage. Above 9 km there was a high frequency of stratospheric CO values with typical mixing ratios in the 50 ppbv or less range.

In Figure 2c, NO increases dramatically north of 20°N in the 0-4 km altitude range. North of 30°N, the average value appears to drop by nearly a factor of 2. For intermediate altitudes (4-8 km) a significant decrease in both the variability and average mixing ratio is seen for latitudes north of 30°N. At the highest altitudes (8-12 km) some of the highest mixing ratios of NO observed throughout the entire mission are seen over the latitude interval of 20-30°N. Although high values are also seen north of 30°N for this altitude range, it is important to note that these high NO mixing ratios are not coincident with the high CO values observed. Instead, the high CO values are correlated with unusually high PAN levels

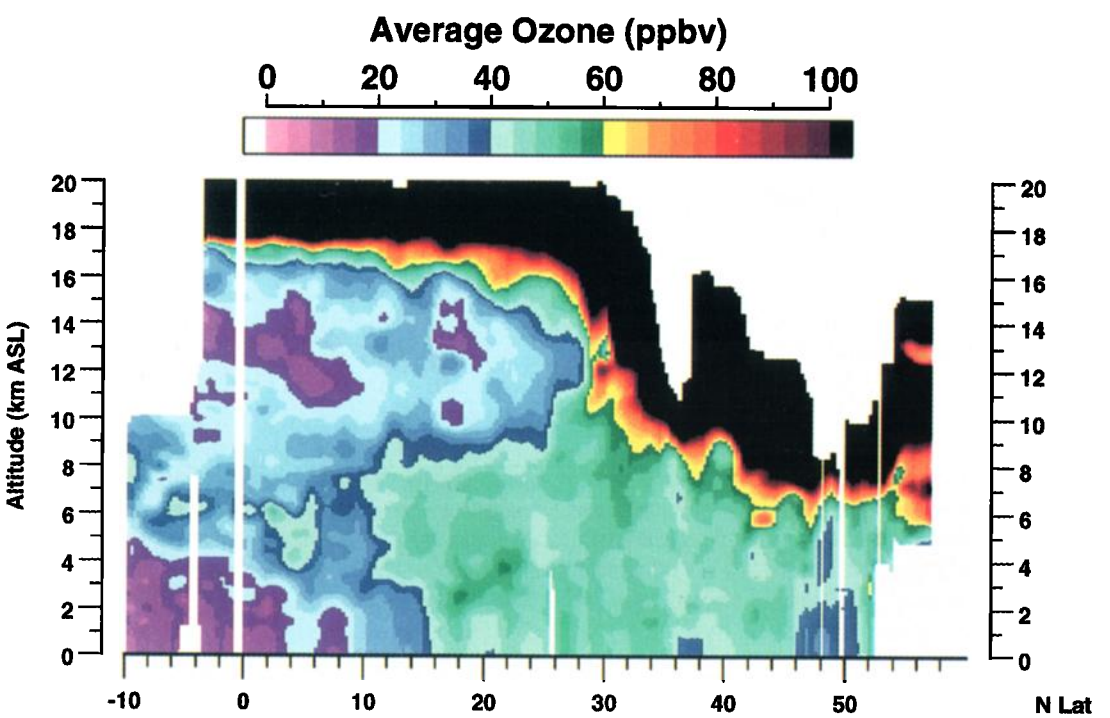

Plate 1. Composite UV-DIAL latitude-altitude O_3 distribution. Low-altitude values (below 1.5 km) were extrapolated to the surface using in situ O_3 data.

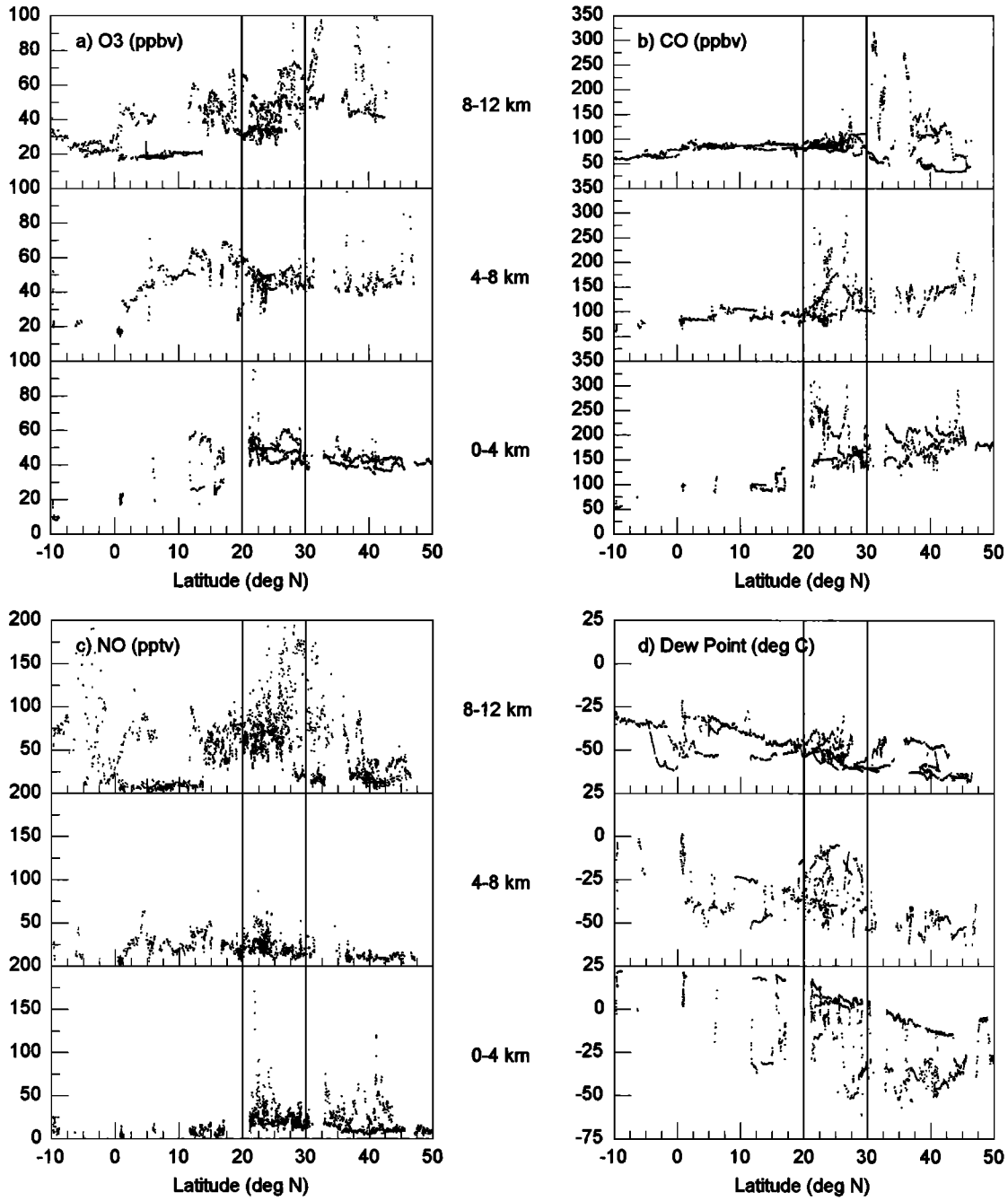

Figure 2. Latitudinal distributions of (a) O_3, (b) CO, (c) NO, (d) dew point, (e) C_2H_6, and (f) C_3H_8 for the altitude ranges of 0-4, 4-8, and 8-12 km.

approaching 1 ppbv; whereas, PAN levels less than 100 pptv were observed for periods of elevated NO. As expected, Figure 2d shows decreasing values for the dew point as more northern latitudes are reached. Like CO, the trends in NMHCs, as shown in Figures 2e and 2f, reveal abrupt increases when moving from tropical to extratropical latitudes and steadily increase with latitude north of 20°N. Unlike CO, however, there appears to be an absence of extreme values for NMHC's in the latitude range of 20-30°N.

Figures 3a-3f give the median observations as a function of altitude for the extratropical regimes of 20-30°N and 30-50°N. These values were used in time-dependent model calculations discussed later in the text. No median values are shown for the 30-50°N latitude range above 8 km because the tropopause height at these latitudes was only 8-9 km. The median data in these figures clearly show that the trends in CO and O_3 are very modest relative to those for NO and H_2O. For example, both NO and H_2O exhibit gradual changes with altitude at 20-30°N; whereas, for altitudes above 2 km they undergo a sudden decrease at 30-50°N.

The most striking difference in the median values for the two latitude regimes are those displayed by the NMHC species (figures 3e and 3f). Both C_2H_6 and C_3H_8 are significantly elevated for 30-50°N relative to 20-30°N. This most

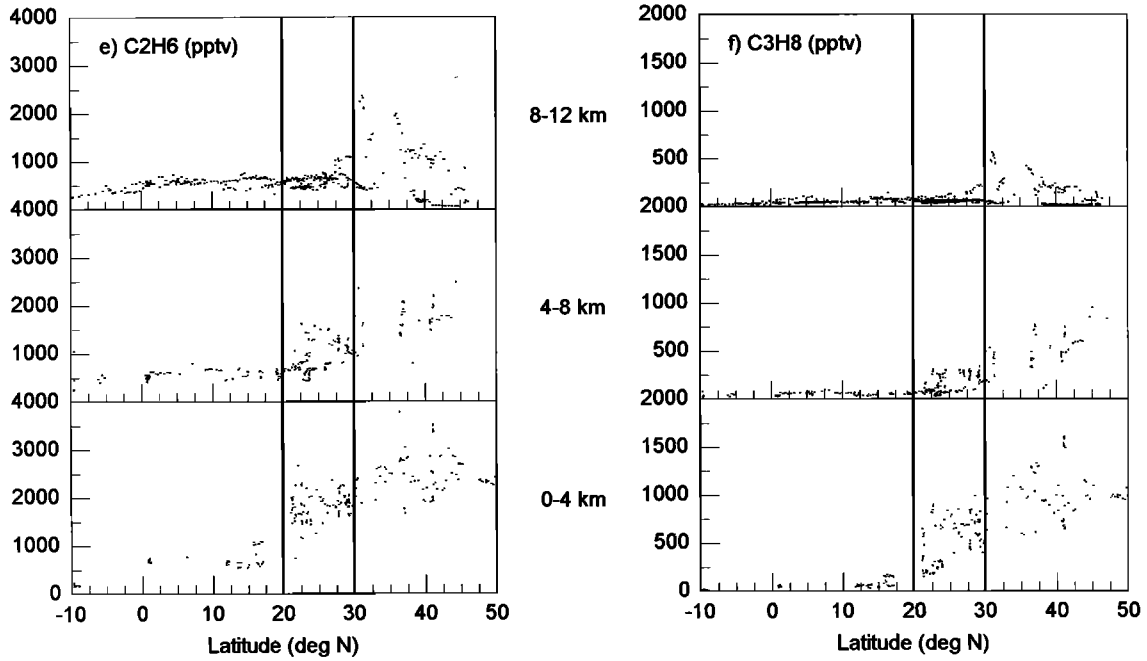

Figure 2. (continued)

likely reflects greater continental outflow at the higher latitudes; however, another contributing factor could be the longer photochemical lifetime for NMHCs north of 30°N. Recall, there was a difference in median total O_3 of ~150 Dobson units between the two regimes. The impact of this shift on the level of photochemical activity is discussed in detail in section 3.3.

While the PEM-B data were not formally segregated longitudinally, they were examined for evidence of long range transport of pollutants into the open Pacific from the Pacific Rim. For the 20-30°N sampling regime the bulk of the data were collected during six flights covering a longitudinal range of 115° to 165°E. Altitudes for which the sampling covered the greatest longitudinal range were 0-1 and 8-10 km; however, even at these two altitudes major longitudinal gaps existed. In the case of 0-1 km, continental pollution in the form of elevated NO levels was found to be quite evident near 120°E, just off the coast of Taiwan; however, relatively high BL values (e.g., 20-40 pptv) persisted out to 145 and 165°E, a distance of more than 2000 km from the Asian Pacific Rim. Similarly, near the coast of Taiwan, CO mixing ratios of 250 ppbv were recorded, but again values in the 150-175 ppbv range were observed at 145 and 165°E. The latter observations at 165°E were all from flight 16, a flight that was specifically intended to sample the extent to which continental outflow behind a front could move out into the Pacific. Thus, the above findings clearly demonstrate that anthropogenic emissions of O_3 precursors can extend far out into the Pacific at this time of year.

3. Data Analysis

3.1. Ozone Photochemistry

The critical photochemical processes that control the rate of formation and destruction of O_3 have been previously discussed [*Davis et al.*, 1996; *Crawford et al.*, this issue] and are summarized in Table 2. On the basis of these reactions the photochemical formation and destruction of ozone can be defined as

$$F(O_3) = \{k_4[HO_2]+k_5[CH_3O_2]+k_6[RO_2]\}[NO] \quad (1)$$

$$D(O_3) = k_3[O(^1D)][H_2O]+\{k_7[OH]+ k_8[HO_2]\}[O_3] \quad (2)$$

The net effect of all photochemical processes on O_3 (the photochemical ozone tendency) can then be defined as the difference between formation and destruction.

$$P(O_3) = (\{k_4[HO_2] + k_5[CH_3O_2] + k_6[RO_2]\}[NO]) - (k_3[O(^1D)][H_2O] + \{k_7[OH] + k_8[HO_2]\}[O_3]) \quad (3)$$

From a chemical point of view, equation (3) is most appropriate for remote global regions involving low to modest levels of NO_x (e.g., <500 pptv). As noted by other authors [e.g., *Chameides et al.*,1987; *Liu*, 1977], under these conditions the additional O_3 loss reaction sequence defined by (R10) and (R12) is insignificant. For much higher levels of NO_x, (R10) and (R12) result in an additional destruction term in equation (3):

$$k_{10}[NO][O_3](k_{12}[NO_2][OH]/\{J_{11}[NO_2]+k_{12}[NO_2][OH]\}) \quad (4)$$

3.2. Model Description

All O_3 photochemical evaluations presented in this analysis have been based on output from a time-dependent (TD) photochemical box model. Details concerning this model have been previously described by *Davis et al.* [1993, 1996] and *Crawford et al.* [this issue]. Specifically, this model was used to calculate diurnal profiles for both radical species and the modeling products $F(O_3)$, $D(O_3)$, and $P(O_3)$. As noted earlier in the text, input used to constrain the model consisted of median values for O_3, CO, H_2O, NO, and NMHCs for

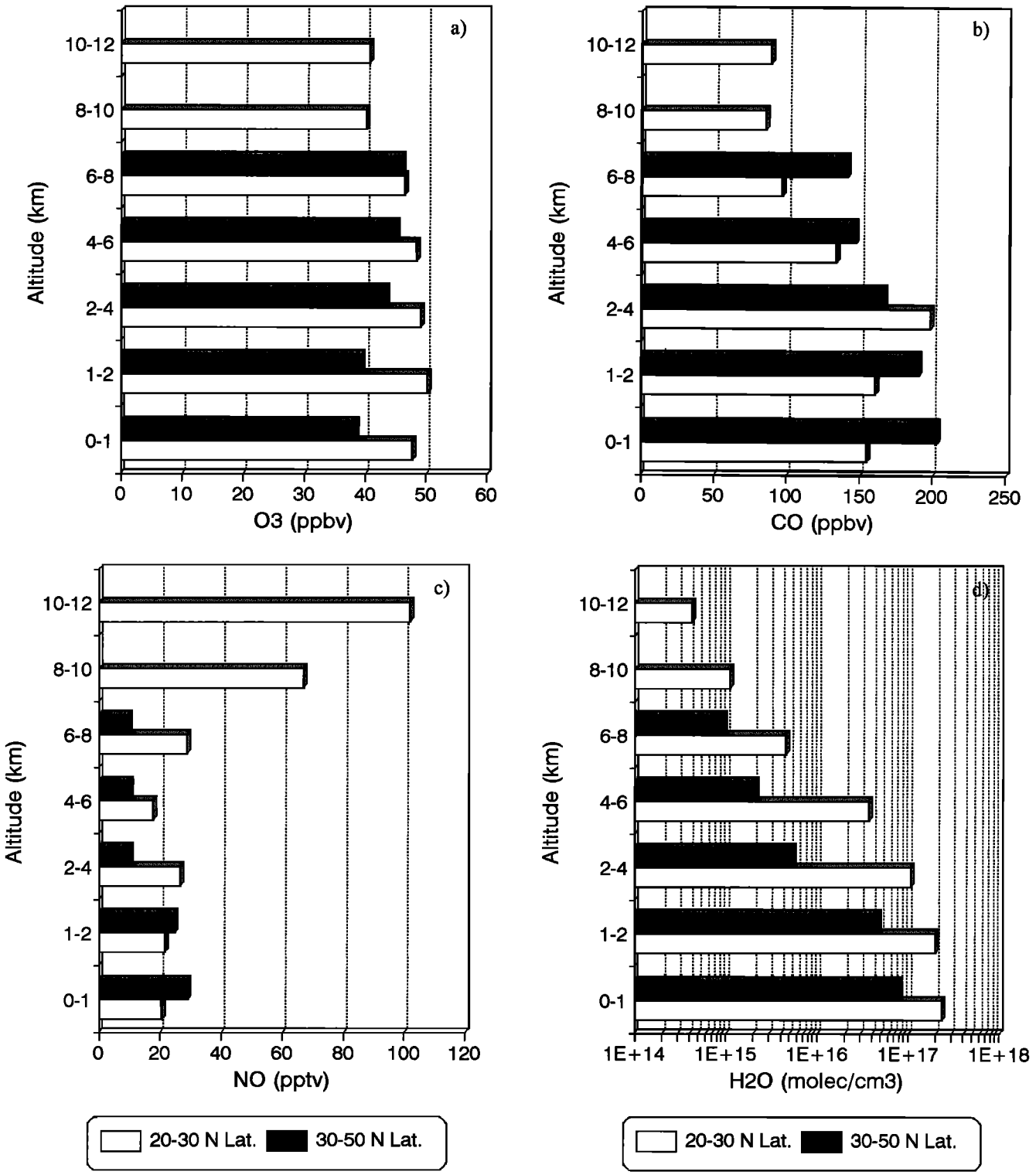

Figure 3. Median altitude distributions of (a) O_3, (b) CO, (c) NO, (d) H_2O, (e) C_2H_6, and (f) C_3H_8 for the latitude ranges of 20-30°N and 30-50°N.

specific altitude/latitude bins (see Figures 3a-3f) as well as median values for the parameters listed in Table 1. With the exception of NO, all variables were assumed to be constant over a 24-hour period. In the case of NO, the source flux was adjusted to match the median NO value.

The initial values for all photolysis rates (J-values) were those calculated for clear-sky conditions using a two-stream radiative transfer model (see *Crawford et al.*, 1996 and references therein). J-values were then further adjusted to simulate actual solar/cloud conditions encountered during sampling using a cloud correction factor (CCF) based on in-flight UV measurements from both an Eppley radiometer and a $J(NO_2)$ radiometer [*Junkerman et al.*, 1989]. Both instruments, however, exhibit a systematic difference from the two-

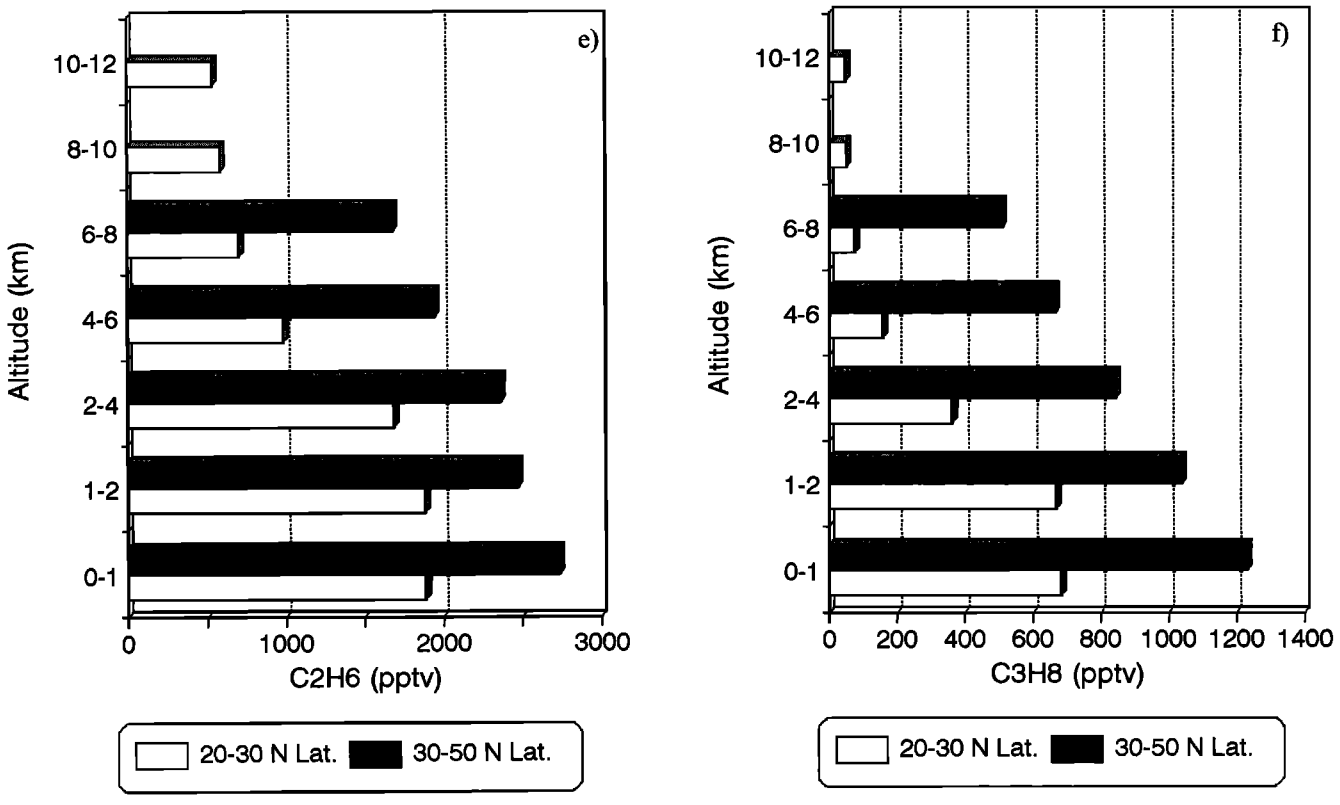

Figure 3. (continued)

stream model calculations for clear-sky flight periods. This problem was first documented during PEM-A [*Crawford et al.*, 1996] with the further complication that these differences have changed considerably between past NASA-GTE campaigns. Furthermore, the range in these systematic differences (e.g., factors of 1.04 to 1.53) has been too large to justify through any natural differences in atmospheric conditions such as aerosol loading. This inconsistency has led to an additional correction for these data which has involved normalizing the radiometer data with the clear-sky radiometer-to-model ratio. For PEM-B this ratio was determined to be 1.53. This normalization allows for corrections due to cloud variability without allowing the systematic difference to impact on the model calculations. It also adds consistency to comparisons between results for different NASA-GTE campaigns such as that presented here with those from PEM-A which had a clear-sky radiometer-to-model ratio of 1.35. The normalized median CCF values used to constrain the TD model for the current set of calculations are listed in Table 3.

To evaluate the potential magnitude of any systematic error in model calculations related to rate constant uncertainties, we have performed Monte Carlo calculations similar to those described by *Thompson and Stewart* [1991] and also reported by *Davis et al.* [1993]. These calculations have assumed uncertainties in gas phase and photolytic reactions as specified by *DeMore et al.* [1994]. Since many of these uncertainties are temperature dependent, calculations were performed for median conditions for two different altitude ranges (i.e., 0-1 and 10-12 km) within the 20-30°N regime. Results of these calculations showed that the 1σ potential systematic error for HO_2 should be within ±18% and ±35% for 0-1 and 10-12 km, respectively. Similarly, the potential systematic error in $F(O_3)$ should be within ±23% and ±38%, and for $D(O_3)$ it should be within ±28% and ±64%.

Table 2. Ozone Photochemistry

(R1)	$O_3+h\nu \rightarrow O(^1D)+O_2$
(R2)	$O(^3P)+O_2 \rightarrow O_3$
(R3)	$O(^1D)+H_2O \rightarrow 2OH$
(R4)	$HO_2+NO \rightarrow NO_2+OH$
(R5)	$CH_3O_2+NO \rightarrow NO_2+CH_3O$
(R6)	$RO_2+NO \rightarrow NO_2+RO$
(R7)	$O_3+OH \rightarrow HO_2+O_2$
(R8)	$O_3+HO_2 \rightarrow OH+2O_2$
(R9)	$HO_2+HO_2 \rightarrow H_2O_2+O_2$
(R10)	$NO+O_3 \rightarrow NO_2+O_2$
(R11)	$NO_2+h\nu \rightarrow NO+O(^3P)$
(R12)	$NO_2+OH+M \rightarrow HNO_3$

3.3. Formation, Destruction, and Tendency of O_3

Modeling results for $F(O_3)$, $D(O_3)$, and $P(O_3)$ are shown in Table 4. Values cited here are diurnal average rates. For

Table 3. Cloud Correction Factors

Altitude, km	20-30°N	30-50°N
0-1	0.78	0.64
1-2	0.83	0.77
2-4	0.89	0.92
4-6	1.04	0.93
6-8	1.14	0.93
8-10	1.18	
10-12	0.97	

Table 4. Diurnal Averaged Rates for O_3 Formation, Destruction, and Tendency

	Latitude Range, 20-30°N				Latitude Range, 30-50°N			
Altitude Range, km	$F(O_3)$, molec/cm^3/s	$D(O_3)$, molec/cm^3/s	$P(O_3)$, molec/cm^3/s	$P(O_3)$, ppbv/day	$F(O_3)$, molec/cm^3/s	$D(O_3)$, molec/cm^3/s	$P(O_3)$, molec/cm^3/s	$P(O_3)$, ppbv/day
0-1	1.01E+06	8.15E+05	1.94E+05	0.68	3.63E+05	9.55E+04	2.67E+05	0.88
1-2	9.88E+05	8.04E+05	1.84E+05	0.72	3.43E+05	9.36E+04	2.49E+05	0.93
2-4	9.51E+05	6.09E+05	3.42E+05	1.54	7.34E+04	4.36E+04	2.98E+04	0.13
4-6	3.67E+05	2.99E+05	6.75E+04	0.37	5.99E+04	3.36E+04	2.64E+04	0.14
6-8	2.10E+05	8.11E+04	1.29E+05	0.93	3.95E+04	2.01E+04	1.94E+04	0.24
8-10	2.32E+05	3.18E+04	2.00E+05	1.85				
10-12	1.56E+05	1.58E+04	1.40E+05	1.61				

Read 1.01E+06 as 1.01×10^6.

both regimes the values of $F(O_3)$ and $D(O_3)$ decrease with altitude, reflecting in large part reductions in H_2O levels with altitude. Even so, O_3 formation rates for 20-30°N exceed those for 30-50°N for all altitudes examined. The magnitude of this difference varies with altitude being nearly a factor of 3 for 0-1 km, but ranging up to factors of 5 to 13 at altitudes of 2-8 km. The difference in O_3 destruction is even more pronounced with 20-30°N exceeding 30-50°N by a factor of 8.5 at 0-1 km and factors of 4 to 14 at altitudes of 2-8 km. These dramatic differences in both $F(O_3)$ and $D(O_3)$ have been found in large part to be due to the highly reduced actinic flux calculated for the 30-50°N regime. This reduction is primarily a result of the large increases in the total overhead O_3 column density. Model simulations indicate that nearly two-thirds of this difference can be attributable to differences in total overhead O_3 with the remaining one-third coming from differences due to shifts in latitude (e.g., solar zenith angle) and the degree of cloudiness (see Table 3). Figure 4 compares model-calculated diurnal-average rates for production of $O(^1D)$ (i.e., $J(O^1D)$) for each regime. Photolysis rates for 20-30°N are shown to be 5-10 times greater than those for 30-50°N.

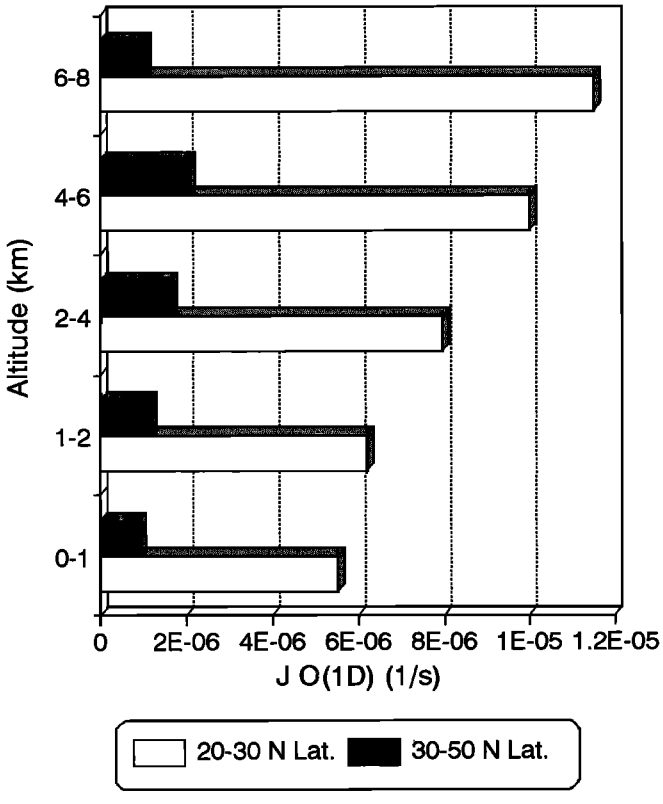

Figure 4. Altitude distribution of $J(O^1D)$ calculated for the latitude ranges 20-30°N and 30-50°N.

Although Table 4 indicates that major differences exist between the two regimes for $F(O_3)$ and $D(O_3)$, the results for $P(O_3)$ show that both regimes exhibit net photochemical O_3 production at all altitudes. This finding is quite surprising in that previous studies have typically found that the marine boundary layer and the lower free troposphere are regions of net O_3 destruction [*Chameides et al.*, 1987; *Davis et al.*, 1996; *Chen*, 1995; *Jacob et al.*, 1996; *Crawford et al.*, this issue]. It can be argued that within the uncertainties associated with the Monte Carlo calculations described earlier that $P(O_3)$ at 20-30°N below 4 km could in fact be slightly negative. Nonetheless, any such systematic error in reaction rates would similarly impact earlier assessments and does not diminish the importance of the differences between these results and those of earlier marine studies

4. Discussion

4.1. Ozone Chemical Controlling Factors

Figure 5 shows the magnitude of the different reaction channels contributing to the photochemical destruction and formation of O_3 as represented by equation (3). For the latitude range 20-30°N and an altitude of 0-1 km (Figure 5a), formation is dominated by reaction (R4), HO_2+NO, (e.g., 60%). The importance of this process increases with altitude reaching 84% at 10-12 km. This shift primarily reflects the steady decrease in the relative importance of peroxy radicals as derived from the oxidation of CH_4 and NMHCs. At the lowest altitudes NMHCs account for only a very modest contribution to $F(O_3)$ with reaction (R6) contributing 20% at 0-1 km, decreasing to 10% at altitudes <4 km. The contribution from NMHCs was dominated by $\geq C_4$ alkanes and aromatics which collectively accounted for 70-80% of the RO_2 formed, and hence 70-80% of the RO_2+NO reaction rate. For 30-50°N (Figure 5b), $F(O_3)$ is also dominated by reaction (R4), which accounts for 60-70% of the total at all altitudes. NMHCs play a somewhat larger role in defining the value of $F(O_3)$ for the 30-50°N regime, contributing 20% from 0-4 km and ~10% at all other altitudes. Again, 70-80%

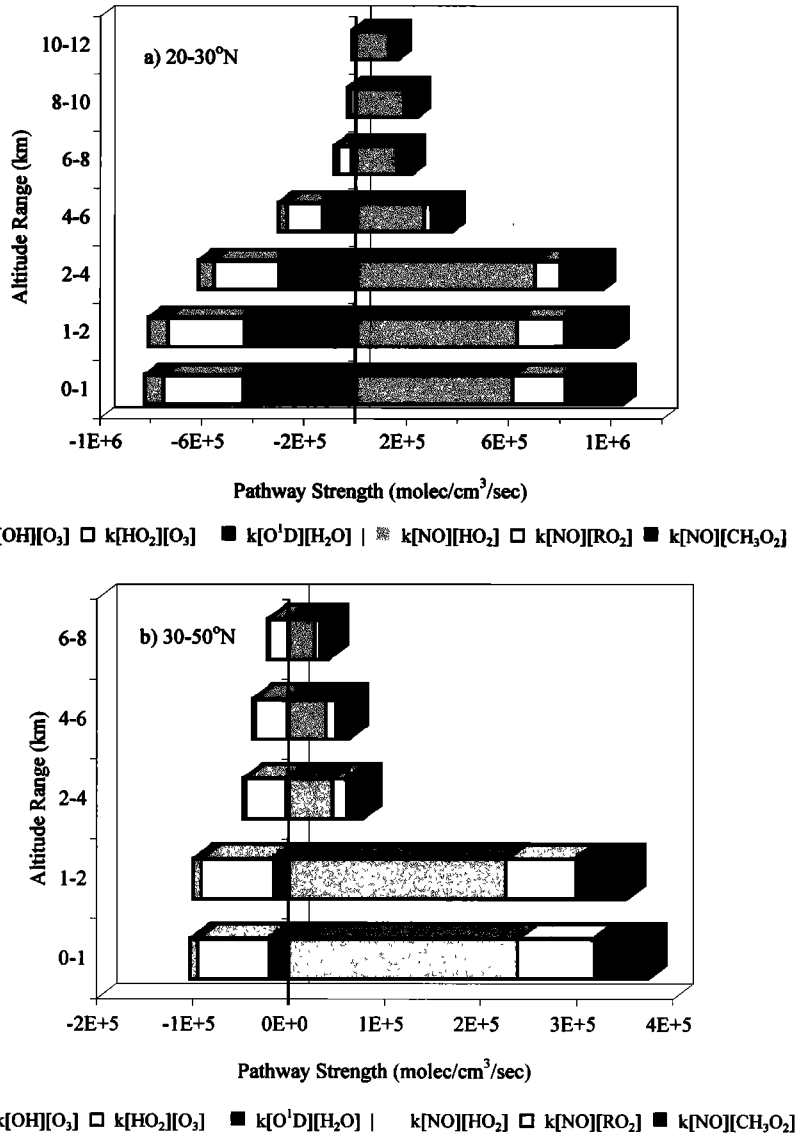

Figure 5. O_3 destruction and formation pathways for the latitude ranges of (a) 20-30°N and (b) 30-50°N.

of the NMHC contribution was from $\geq C_4$ alkanes and aromatics.

$D(O_3)$ for 20-30°N and altitudes below 4 km (Figure 5a) is dominated by reaction (R3), $O(^1D)+H_2O$; however, reactions (R7) ($OH+O_3$) and (R8) (HO_2+O_3) still make up ~47% of the total. Above 4 km, reaction (R8) becomes dominant reflecting rapid decreases in H_2O levels, but (R7) also increases and on reaching 10-12 km becomes comparable to (R8). At this altitude each is found to contribute ~46%. In no case is any reaction found to define more than 60% of the total destruction rate, and typically the contribution is less than 50%. By contrast, O_3 destruction at 30-50°N (Figure 5b) is dominated by reaction (R8) at all altitudes (e.g., 73-89%). Also at these latitudes, the sharp reduction in $O(^1D)$ due to reduced actinic flux limits the importance of reaction (R3) to less than 20% at all altitudes.

The importance of specific elementary reactions to ozone photochemistry can only be evaluated using a photochemical box model. It is also important to explore the extent to which O_3 formation and destruction can be understood in terms of simpler empirical equations based only on measured chemical and radiative parameters. In earlier work reported by *Davis et al.* [1996], two empirical equations were developed to see if model-calculated diurnal-average rates of O_3 destruction and formation could be related to the critical variables O_3, H_2O, and NO_x.

$$D(O_3) = 1.03 \times 10^5 \left(\frac{O_3}{M}\right)[H_2O]^{.767} \quad (5)$$

$$F(O_3) = \left(\frac{NO_x}{M}\right)(2.87 \times 10^{17} \ln\left(\frac{H_2O}{O_3}\right) - 2.47 \times 10^{18}) \quad (6)$$

where $D(O_3)$ and $F(O_3)$ have units of ppbv/day, O_3 has units of ppbv in equation (5) and molecules/cm^3 in equation (6), H_2O and M have units of molecules/cm^3 in both equations, and NO_x has units of pptv.

These equations were based on model calculations for the 13 altitude/latitude sampling bins from PEM-A. Adding

PEM-B model calculations for the tropics [*Crawford* et al., this issue] and extratropics (See Table 4), this database is expanded to 37 altitude/latitude sampling bins. When applied to the expanded database, equation (5) was successful in predicting $D(O_3)$ values to within ± 50% for all cases but five, all of which were in the PEM-B 30-50°N regime. Application of equation (6) proved to be considerably less successful. In this case, not only were the predictions for 30-50°N significantly in error, but those for some high-altitude data bins even generated negative values.

That these equations were unable to predict reasonable values of $F(O_3)$ and $D(O_3)$ for the 30-50°N latitude regime is quite understandable since they contained no variable which could account for large changes in radiative conditions. Recall that it was in this latitude zone that a major enhancement in total overhead O_3 column density was observed. Expanding the earlier relationship to account for large changes in radiative conditions requires one to address not only changes in O_3 column density but also seasonal effects, latitude changes, shifts in daily solar insolation, and variations in cloud conditions. Estimating the impact of clouds requires the use of a model; however, O_3 column density and seasonal/latitudinal changes in solar insolation can be more easily incorporated into empirical equations of the type of (5) and (6). For O_3 column density the variable "TOMS" was adopted signifying the use of data derived from the Total Ozone Mapping Spectrometers which have been placed in orbit on a number of satellites (e.g., Meteor-3, Nimbus-7, etc.). To account for seasonal/latitudinal impacts, the cosine of the high noon solar zenith angle (θ_{HN}) was adopted. This value is easily calculated given only the latitude and day of the year.

Incorporating these new variables, the following updated version of equation (5) was developed.

$$D(O_3) = 1.03 \times 10^{-1} \frac{[O_3][H_2O]^{0.6}\cos(\theta_{HN})}{TOMS} \quad (7)$$

Here $D(O_3)$ is in ppbv/day, O_3 is in ppbv, H_2O is in ppmv, and TOMS is in Dobson units. Both equations (5) and (7) illustrate the linear dependence of $D(O_3)$ on O_3 and the near square root dependence on H_2O. The linear dependence on O_3 comes from the fact that it appears explicitly in two O_3 destruction terms (see Equation 2) and is linearly related to the concentration of $O(^1D)$ in the remaining term. The sublinear dependence on H_2O is a result of its explicit appearance in only one term. HO_x ($OH + HO_2$) radicals in the other terms are indeed derived from H_2O; but increases in H_2O do not typically result in linear increases in HO_x. The $\cos(\theta_{HN})$/TOMS term indicates a linear influence from radiative conditions which directly impacts on the production of $O(^1D)$ through O_3 photolysis.

A correlation plot of $D(O_3)$ determined from equation (7) versus model-estimated values is shown in Figure 6a. This equation predicted $D(O_3)$ to within ±25% for 30 of the 37 model calculations. Of the remaining seven, all but two were within ±50%. The worst source of error came from those bins associated with the 0-1 and 1-2 km data for 30-50°N. In this case the errors were +150 and +80%, respectively. A large part of the latter discrepancy appears to be the result of not including a variable that deals with cloudiness.

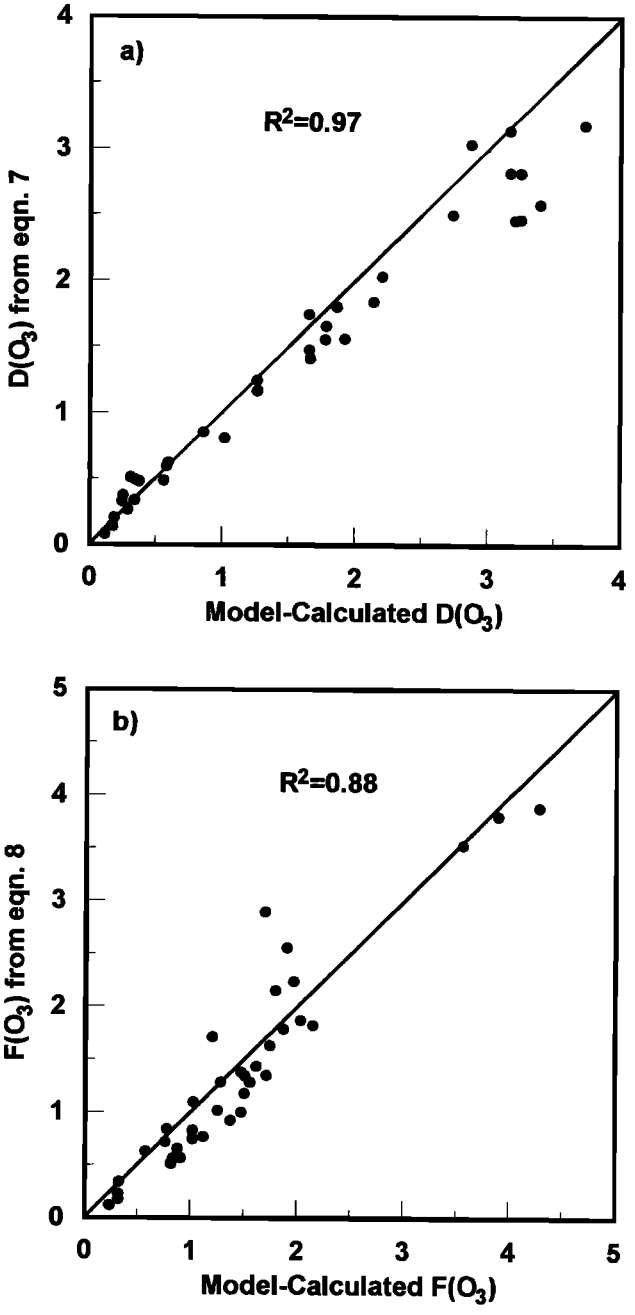

Figure 6. Empirically derived values of (a) $D(O_3)$ and (b) $F(O_3)$ versus model-calculated estimates.

A further modification of the empirical equation for $F(O_3)$ resulted in the following form:

$$F(O_3) = 2.19 \times 10^{7}[NO]\sqrt{\frac{[H_2O][O_3]\cos(\theta_{HN})}{[M]TOMS}} \quad (8)$$

Here $F(O_3)$ is in ppbv/day, NO is in pptv, O_3 is in ppbv, H_2O is in ppmv, M is in molecules/cm^3, and TOMS is in Dobson units. The form of equation (8) reflects the fact that $F(O_3)$ should be proportional to the product of NO and peroxy radicals. Since peroxy radicals are derived primarily from the OH oxidation of CO and hydrocarbons, the square root terms

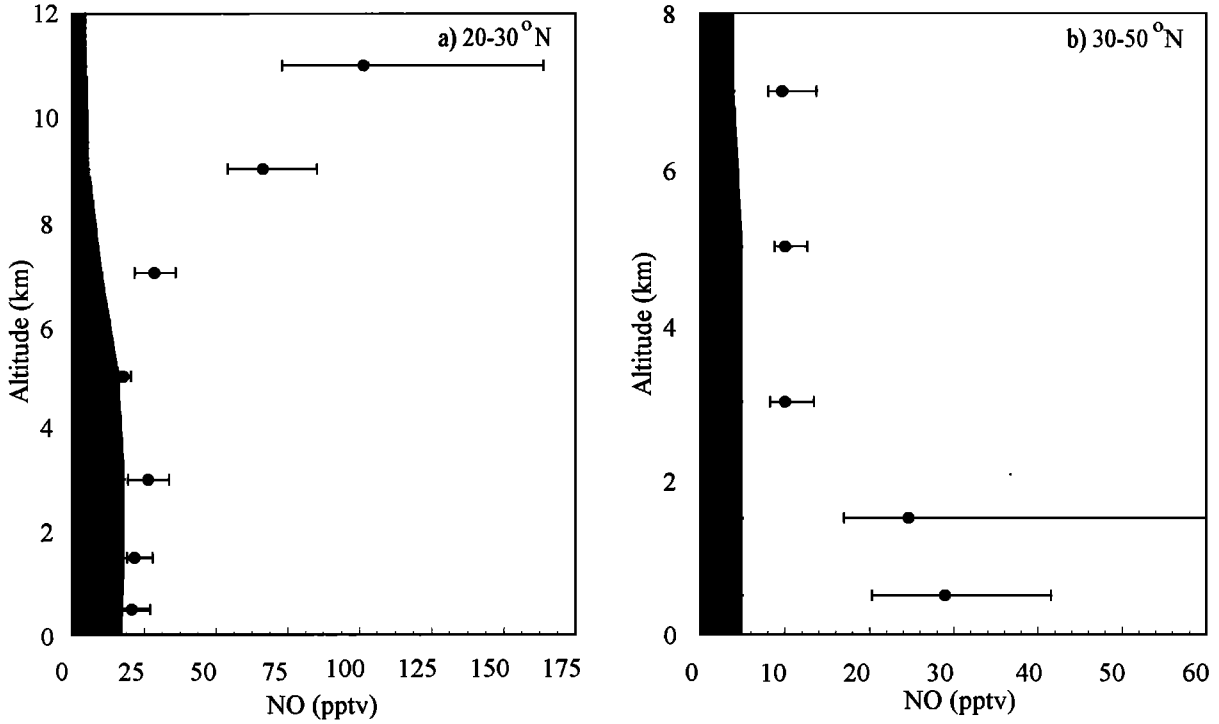

Figure 7. Critical NO (shaded area) and median measured NO (symbols) versus altitude for (a) 20-30°N and (b) 30-50°N. Error bars encompass the inner quartiles.

represent the production of $O(^1D)$ from O_3 photolysis and the fraction of $O(^1D)$ reacting with H_2O to create OH versus being collisionally quenched. The square root dependence of these terms reflect the loss of peroxy radicals through self reactions of the (R9) type.

Figure 6b shows a correlation plot of $F(O_3)$ as evaluated from equation (8) versus that estimated from box model runs. This equation predicted $F(O_3)$ to within $\pm 40\%$ for 33 of 37 model results. Of the remaining four, all but one fell within 50%. In the case of $F(O_3)$, cloud conditions did not cause a major problem due largely to the square root dependence on radiative conditions. However, on average, the uncertainties for $F(O_3)$ were found to be larger than those for $D(O_3)$. This is most likely due to shifts in the importance of NMHCs (e.g., RO_2) which are not accounted for in equation (8).

4.2. Critical NO

Critical NO (NO_{crit}) is defined as the level of NO at which O_3 formation and destruction are in balance (i.e., $P(O_3)=0$). As noted earlier, the net O_3 production observed in the lower troposphere was primarily a result of elevated NO levels from continental outflow. A comparison of NO_{crit} with observed NO can provide a measure of the sensitivity of $P(O_3)$ to small changes in NO. PEM-B simulations using median conditions show that NO_{crit} values ranged from 4-18 pptv. Figure 7 shows NO_{crit} and median observed NO with respect to altitude for both 20-30°N and 30-50°N. What is seen here is that ΔNO (NO_{obs}- NO_{crit}) undergoes major variations within a given regime as a function of altitude and also differs considerably between regimes. For 20-30°N, below 6 km, the difference is quite small (e.g., 10-20%); whereas, above this altitude ΔNO is a factor of 2.5 to 20. For 30-50°N the value of ΔNO over all altitudes is between a factor of 2 to 6, but the largest differences are below 2 km. The latter observation reflects the major impact resulting from continental outflow.

That NO_{crit} values should differ so dramatically between regimes (i.e., 5 versus 20 for altitudes <2 km) raises an interesting question related to what determines these "break even" values? To explore this question we return to equations

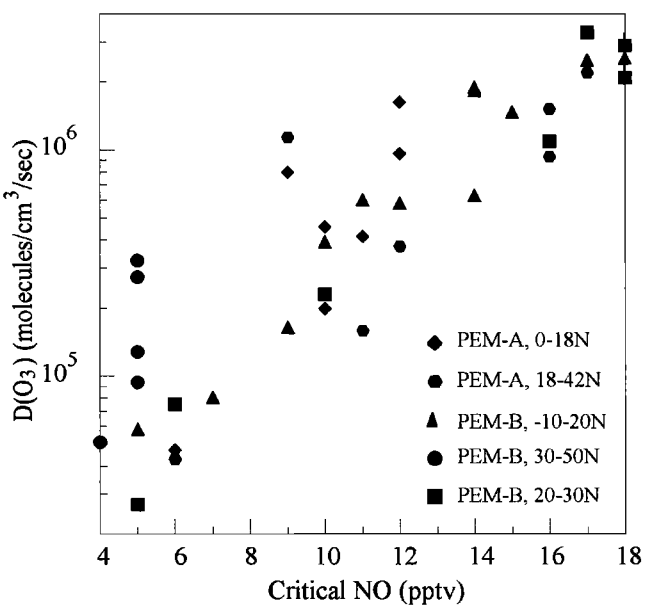

Figure 8. Correlation plot of $D(O_3)$ (log scale) versus critical NO.

(7) and (8) of the previous section. These equations suggest that the trends in NO_{crit} might best be understood in terms of changes in O_3, H_2O, and regional radiative conditions. Each parameter appears in both equations; however, each equation's mathematical dependence on them is quite different. In equation (7), $D(O_3)$ is linearly dependent on both O_3 and radiative conditions with a slightly greater than square root dependence on H_2O. By contrast, equation (8) reveals a square root dependence on all three parameters. This shows $D(O_3)$ to be far more sensitive than $F(O_3)$ to environmental changes as reflected in the values of O_3, H_2O, and radiative conditions.

An examination of the PEM-B data shows no significant variation in median O_3 values with either altitude or latitude, having a range of 38-50 ppbv (see Figure 3a). On the other hand, H_2O exhibits a strong gradient with altitude decreasing by almost three orders of magnitude between 0-1 and 10-12 km. Similarly, a significant latitudinal gradient exists in H_2O, for example, a factor of 3 at 0-1 km and as much as an order of magnitude above 1 km (see Figure 3d). Like H_2O, the levels of $O(^1D)$ also exhibit a strong latitudinal gradient, reflecting changes in the UV solar irradiance and thus in $J(O^1D)$. As shown earlier in Figure 4, this change ranges from a factor of 5 to 10 between 20-30°N and 30-50°N. Given the reduction in H_2O with altitude and both $O(^1D)$ and H_2O with latitude, both O_3 formation and destruction are seen to decrease (e.g., see Table 4); however, the largest decreases occur in $D(O_3)$. This leads to much lower values of NO_{crit} for the 30-50°N regime and, more generally, for high altitudes in both regimes. This point is further demonstrated in a correlation plot of $D(O_3)$ versus NO_{crit} as shown in figure 8. The results reveal a strong trend between these quantities with $R^2=0.78$. The large amount of scatter in the plot most likely reflects the fact that there are still other factors that also impact to some degree on NO_{crit} trends. For example, variations in the levels of CO, NMHCs, etc. are unaccounted for in this simplified view.

4.3. Ozone Budgets

Diurnal-average column-integrated rates of O_3 destruction, formation, and tendency for 20-30°N and 30-50°N are shown in Figures 9a-9c. Also given in each figure legend is the total tropospheric column-integrated rate. Model results show $F(O_3)$ for the 20-30°N regime ($58x10^{10}$ molecules/cm^2/s) to be more than an order of magnitude greater than the average NH stratospheric flux of ~$5x10^{10}$ [*Gidel and Shapiro*, 1980; *Mahlman et al.*, 1980]. However, given the latitude and season, the local stratospheric flux was likely to be substantially larger than the NH average. Even so, we estimate that it would still fall well short of the value cited for photochemical formation. For 30-50°N, $F(O_3)$ is much smaller (10×10^{10} molecules/cm^2/s). In this case the photochemical source is only a factor of two greater than the average stratospheric flux. This suggests that at 30-50°N the local stratospheric source of O_3 is probably larger than that from photochemistry. Ozone destruction for 20-30°N is about 7 times greater than estimates of the average surface deposition, e.g., $37x10^{10}$ versus $5x10^{10}$ [*Kawa and Pearson*, 1989; *Lenschow et al.*, 1982]; while at 30-50°N, $D(O_3)$ ($3.8x10^{10}$) falls just below values for surface deposition. The cited photochemical destruction rates lead to estimated photochemical lifetimes for the tropospheric O_3 column of 16 and 120 days, respectively, for 20-30°N and 30-50°N.

As noted by *Crawford et al.* [this issue] in their analysis of the PEM-B tropical data and *Davis et al.* [1996] in their analysis of the tropical and extratropical data of PEM-A, the level of photochemical activity within the tropospheric O_3 column can be a strong function of altitude. In the current analysis at 20-30°N, 67% of formation and 77% of the destruction occurred below 4 km. For 30-50°N the corresponding values were 81 and 72% below 4 km. These results suggest that for these latitudes and for wintertime conditions, $F(O_3)$ and $D(O_3)$ are quite sensitive to changes in lower tropospheric conditions. Thus, strong low-altitude Asian continental outflow for the late winter and early spring months can greatly amplify the photochemical impact on local O_3 levels.

Estimates of the net O_3 tendency for 20-30°N and 30-50°N indicate that for the PEM-B sampling period the respective tropospheric O_3 columns increased by $21x10^{10}$ and $6.7x10^{10}$ molecules/cm^2/s. As a percentage change, these rates are approximately 2 and 1% per day, respectively. From a regional/hemispheric perspective, it could be argued that these large net positive values for $P(O_3)$ are what is needed to offset the rather large net negative values observed for the tropics (e.g., $-14x10^{10}$ molecules/cm^2/s) [*Crawford et al.*, this issue]. The possibility that O_3 rich extratropical air is transported into the tropics to balance the net photochemical destruction in the tropics was raised by *Crawford et al.* in their analysis of the PEM-B tropical data as well as by *Davis et al.* [1996] in their analysis of the tropical PEM-A data. If this type of transport were to occur, it obviously would also tend to reduce the impact from photochemical O_3 production on the extratropics.

Given the seasonal climatology of tropospheric ozone (1979-1989) as derived from satellite observations [*Fishman et al.*, 1992], the tropospheric O_3 column in the PEM-B extratropical region should have experienced a seasonal increase of 30-40%. This might lead one to conclude that the estimated photochemical increases of 1 to 2% per day are unrealistically high. On further reflection, however, it is unlikely that these estimated rates could be sustained over any significant period of time. For example, it must be recognized that the PEM-B mission was planned in order to sample the western Pacific Rim region during maximum continental outflow. Thus, the overall levels of precursors (particularly NO and NMHCs) were near a maximum and would be expected to gradually decrease with time, especially in the marine boundary layer. There is also a natural leveling effect that would occur with increasing O_3 concentrations since destruction increases linearly with increasing O_3 but formation increases only by the square root of the O_3 level as illustrated in equations (7) and (8). Additionally, with a steady increase in temperature due to the onset of spring, one would predict increases in H_2O with corresponding higher values of $D(O_3)$ and most likely higher values for NO_{crit}. Concurrent with increases in the critical level of NO, increased levels of OH and longer days would decrease the photochemical lifetime of NO_x. Increasing temperatures would also result in a decrease in the levels of PAN. Under cooler conditions this thermally labile nitrogen species can be advected out over the Pacific and thus serve to sustain elevated levels of NO_x at large distances from the source of NO_x. For all of the above

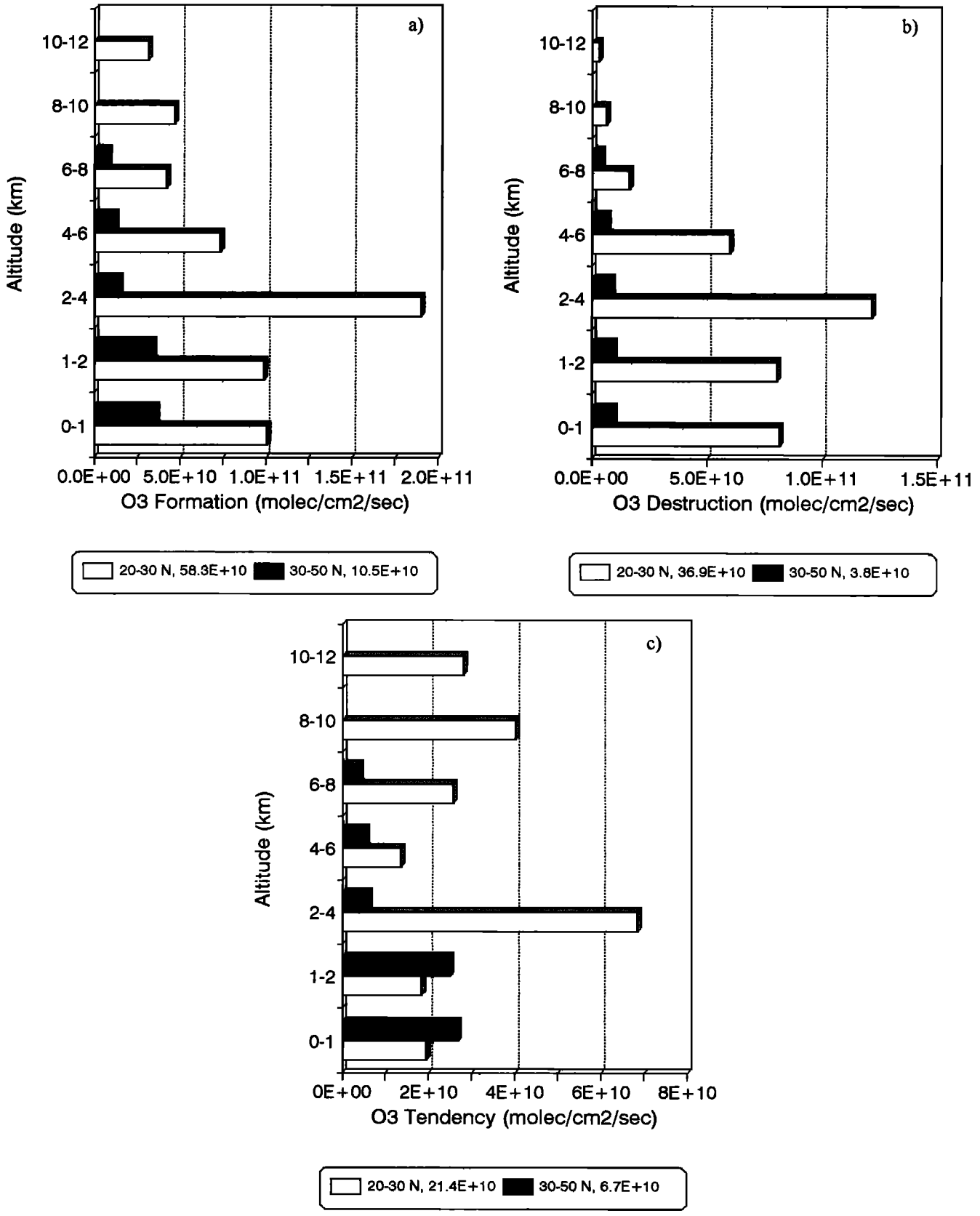

Figure 9. Diurnal-average column-integrated values of (a) $F(O_3)$, (b) $D(O_3)$, and (c) $P(O_3)$. Values are calculated from median conditions for the latitude ranges of 20-30°N and 30-50°N. Total tropospheric column values are annotated at the bottom of the figure.

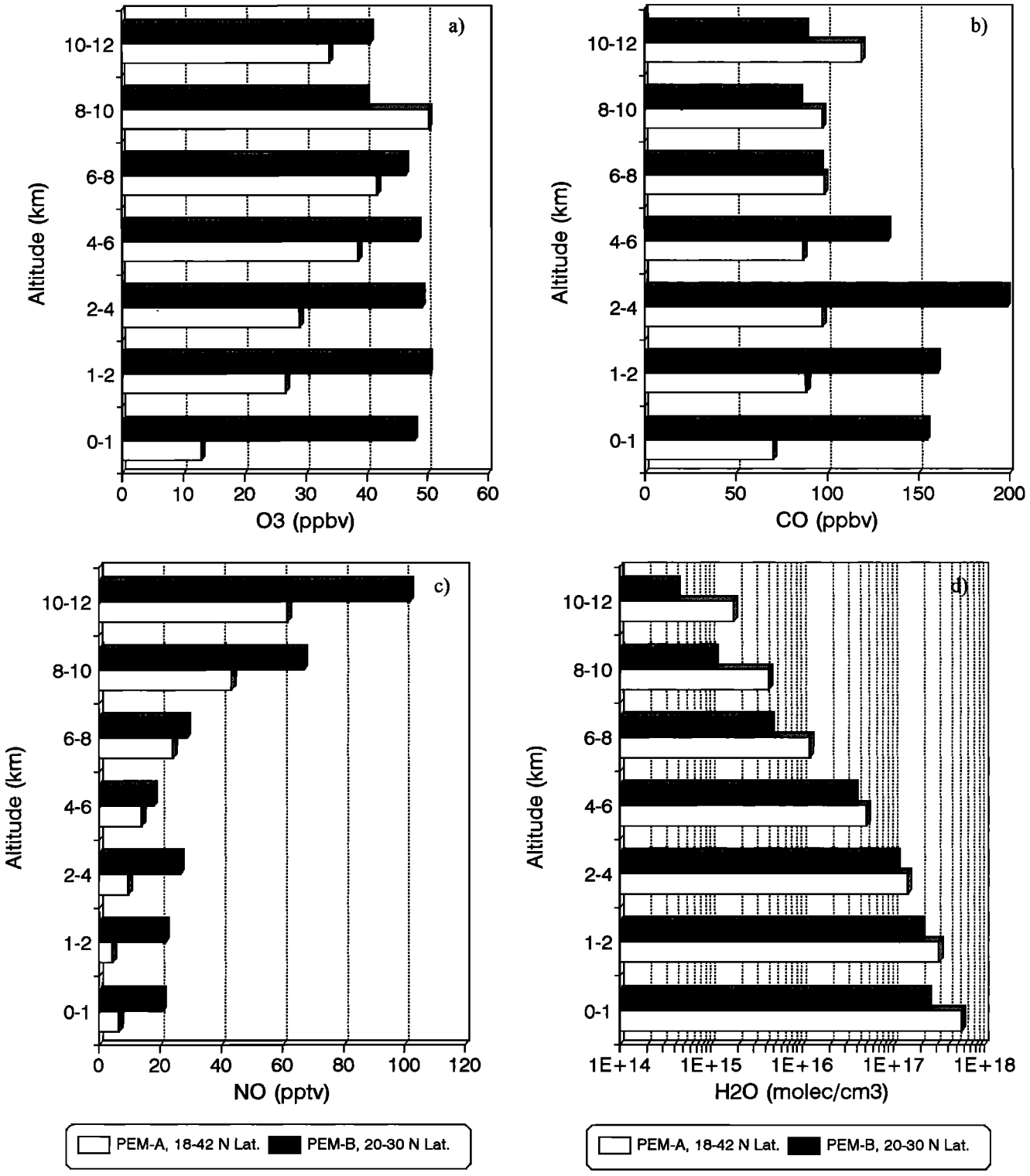

Figure 10. Median altitude distributions of (a) O_3, (b) CO, (c) NO, (d) H_2O, (e) C_2H_6, and (f) C_3H_8 for PEM-West A (18-42°N) and PEM-West B (20-30°N).

reasons, it can be argued that the very high rates of O_3 production estimated for the extratropics based on PEM-B data would be significantly moderated in time. Even so, the above calculations also suggest that under near wintertime conditions, photochemistry in this region of the Pacific can have a very large impact on local and regional O_3 budgets when perturbed by a major outflow of anthropogenic continental emissions.

4.4. Comparison With PEM-A

During PEM-A there was no abrupt drop in the tropopause height at extratropical latitudes. Thus the entire PEM-A

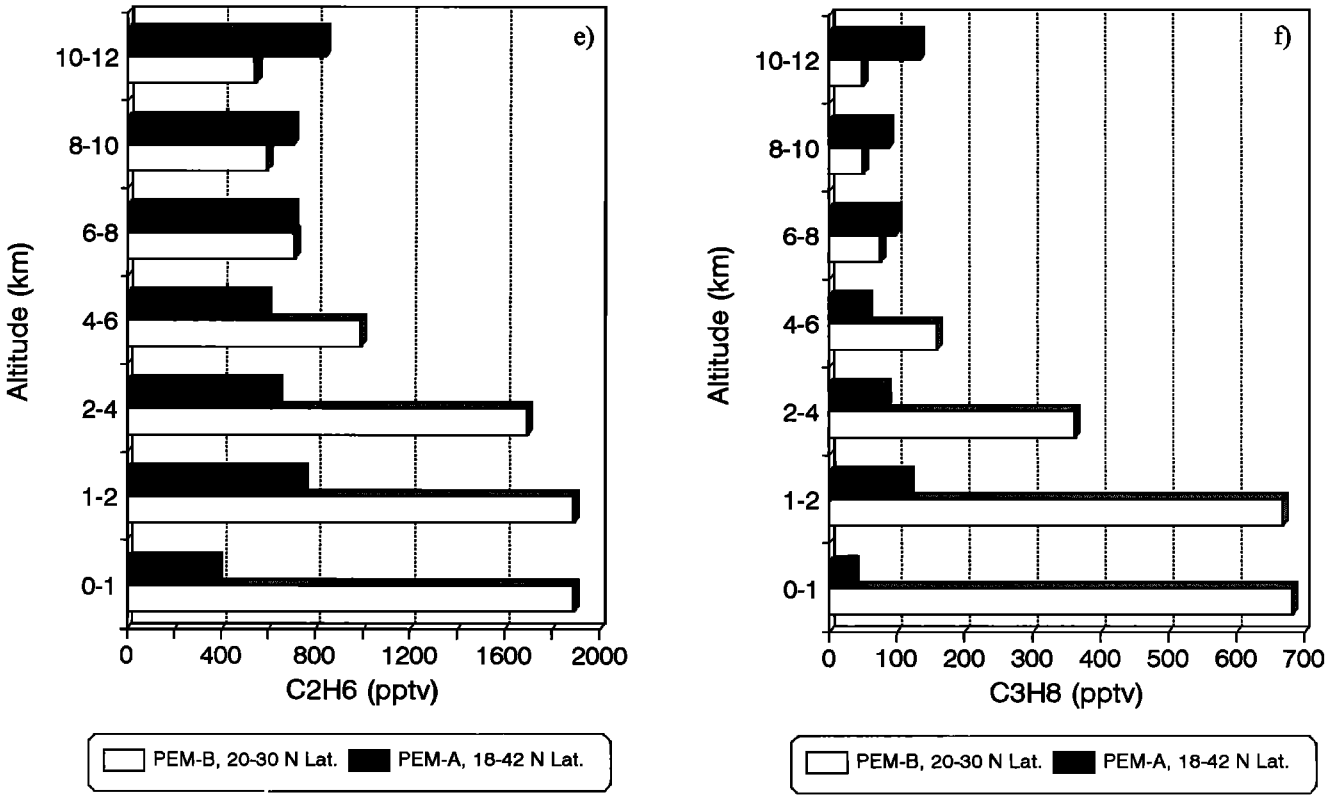

Figure 10. (continued)

region of 18 to 42°N can be characterized as consisting of a single regime [*Davis et al.*, 1996]. This "Pacific Rim" regime was, in fact, not all that dissimilar from the PEM-B 20-30°N sampling region in that nearly 75% of the Pacific Rim PEM-A data were recorded south of 30°N. Most importantly, during PEM-A, no significant latitudinal gradient in the total O_3 column density was present. This is reflected in the observation that for the latitude ranges given, $J(O^1D)$ values were quite similar for both field programs. (Note, both programs took place near solar equinox conditions.)

Figures 10a-10f provide a comparison of several PEM-B (20-30°N) and PEM-A (18-42°N) critical photochemical parameters as a function of altitude. These include median mixing ratio values for O_3, CO, NO, H_2O, C_2H_6, and C_3H_8. Among the differences seen in these data is the contrast in O_3 below 4 km. Ozone levels in PEM-B exceed those in PEM-A by more than a factor of 1.5 and for the BL this difference reaches a factor of 4. This low-altitude enhanced O_3 in PEM-B is a product of the continental outflow of O_3 and its precursors which are still actively producing O_3. This outflow was almost totally absent during PEM-A. Strong evidence of this outflow is also seen in the distributions of CO and NMHCs. At altitudes below 6 km, levels in PEM-B exceed those in PEM-A by factors of 1.5 to 2 for CO, 1.5 to 5 for C_2H_6, and 3 to 20 for C_3H_8. In contrast to this low altitude scenario, above 8 km, PEM-A has only slightly higher CO and NMHC levels. As discussed by *Davis et al.* [1996], the latter observation is in concert with a northern hemisphere, and specifically a Pacific Rim region, that experienced large amounts of deep convection during PEM-A.

A comparison of NO shows PEM-B levels below 4 km exceeding those in PEM-A by factors of 3-5. Even at altitudes above 8 km, PEM-B values still exceed PEM-A values by a factor of approximately 1.5. Observed values for H_2O at high altitude support the view that PEM-A was more influenced by deep convection than PEM-B. Above 6 km PEM-A values are systematically higher by a factor of 2-5 times over those in PEM-B.

Differences in the photochemical O_3 budgets for PEM-A and B are shown in Figures 11a-11c. Rates in these figures are diurnal-average column-integrated values with total tropospheric column rates annotated in each figure legend. The results show that below 4 km O_3 formation in PEM-B exceeds that for PEM-A by a factor of 3. By contrast, above 4 km the difference between PEM-A and B is less than 10%. Overall, this means that O_3 formation in PEM-B exceeded that for PEM-A by nearly a factor of 2. Differences in O_3 destruction are much smaller. PEM-B has slightly larger values in the lower atmosphere, due mostly to higher levels of O_3, but overall the tropospheric column destruction for the two field programs differ by only 15%, PEM-B being greater.

As noted several times earlier in the text, the elevated O_3 formation rate in PEM-B primarily reflects the impact of elevated NO levels from continental outflow. Additionally, however, some enhancement resulted from NMHC oxidation (i.e., $NO+RO_2$). The latter was significantly larger in the case of PEM-B for altitudes below 4 km. This impact is shown more quantitatively in Table 5 which displays the results from several sensitivity calculations for PEM-B. These sensitivity calculations for PEM-B were based on substituting PEM-A median values for NO, CO, or NMHCs. Results show the largest difference generated is that for $F(O_3)$ at low altitudes. For altitudes less than 4 km $F(O_3)$, values during PEM-B would have been 3-4 times lower given PEM-

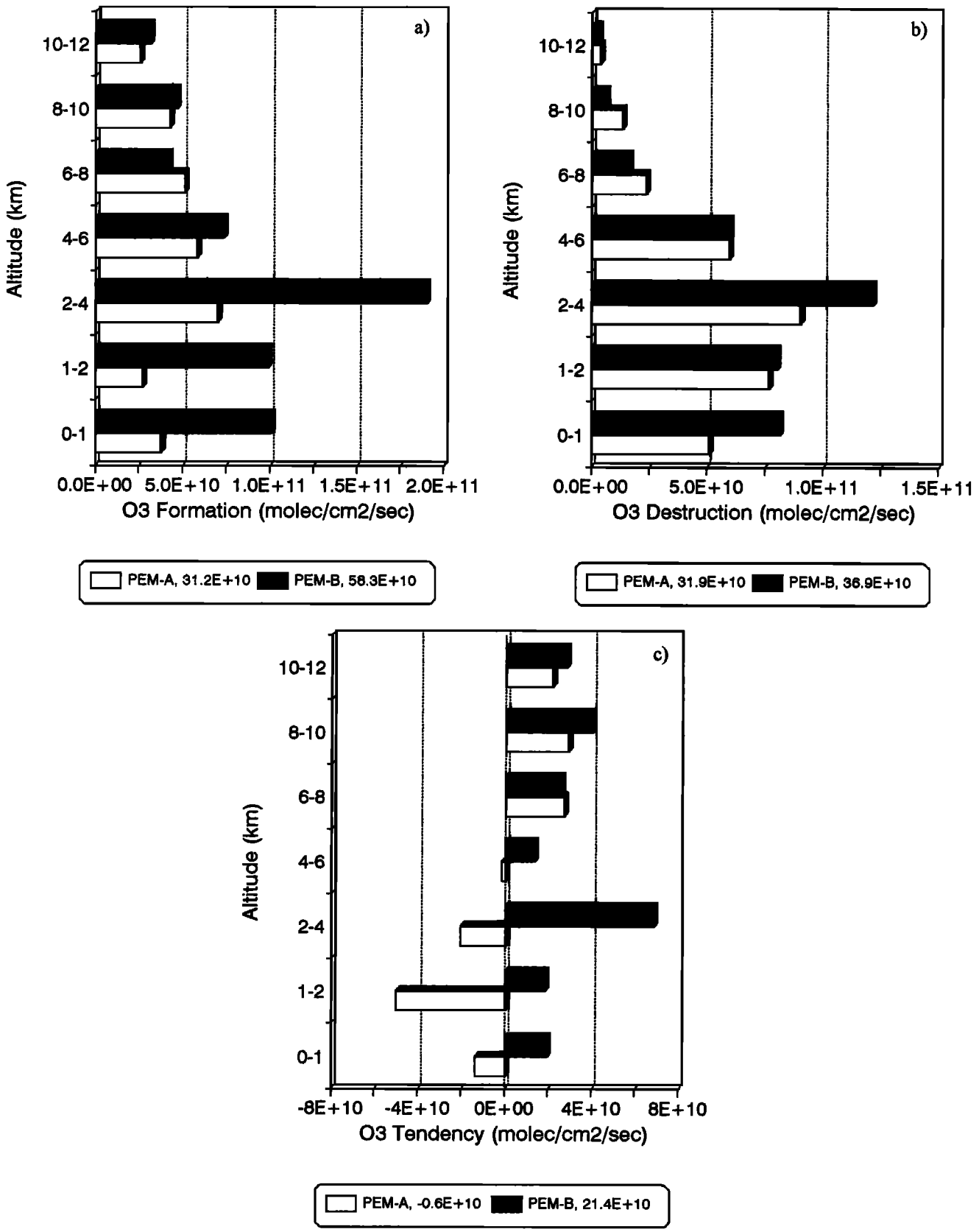

Figure 11. Diurnal-average column-integrated values of (a) $F(O_3)$, (b) $D(O_3)$, and (c) $P(O_3)$. Values are calculated from median conditions for PEM-West A (18-42°N) and PEM-West B (20-30°N). Total tropospheric column amounts are annotated at the bottom of the figure.

Table 5. Sensitivity Calculations for PEM-West B Conditions When Substituting PEM-West A Levels of NO, CO, and NMHCs

	$F(O_x)$ Change			$D(O_x)$ Change		
Altitude	NO	CO	NMHCs	NO	CO	NMHCs
0-1 km	0.37	1.08	0.85	0.94	0.99	1.02
1-2 km	0.25	1.04	0.85	0.93	0.99	1.02
2-4 km	0.39	1.00	0.93	0.96	0.98	1.01
4-6 km	0.79	0.99	0.96	0.99	0.98	1.01
6-8 km	0.86	1.00	1.03	0.99	1.00	1.00
8-10 km	0.72	1.02	1.06	0.96	0.99	1.02
10-12 km	0.73	1.04	1.21	0.96	0.95	1.12

A NO levels. Minor differences are also seen in $D(O_3)$ due to the secondary effects from HO_x levels. For NMHCs the impact on $F(O_3)$ using PEM-A levels is 15% or less. Perhaps the most surprising result is at high altitude (10-12 km) where the NMHC levels of PEM-A resulted in a 21% increase in PEM-B $F(O_3)$ values. Because of the extensive deep convection during PEM-A [*Davis et al.*, 1996], NMHC levels were significantly higher at 10-12 km than in PEM-B. This result makes the point that oxidation of NMHCs at high altitudes can provide a significant source of HO_x as evidenced in the 12% increase in $D(O_3)$. Again, $\geq C_4$ alkanes were the most prominent source of reactive NMHCs. The smallest impact from the substitution of PEM-A input data into PEM-B was found for the variable CO.

When examined in terms of $P(O_3)$, the difference between the two field programs is primarily limited to the lower troposphere with PEM-B showing significant positive values and PEM-A being significantly negative. As previously noted, tropospheric O_3 column rates of formation and destruction are more sensitive to changes in lower atmospheric conditions. For PEM-B, higher NO levels in addition to elevated RO_2 from NMHCs resulted in the net production of O_3.

4.5. NO_x Sources

As is now well documented in the literature, NO_x plays a pivotal role in the photochemical formation of O_3; thus, understanding the NO_x budget is a centrally important issue. The components of this budget include both surface primary sources (i.e., fossil fuel combustion, biomass burning, and soil emission) as well as upper free tropospheric sources (i.e., aircraft emissions, lightning, and stratospheric intrusions). Secondary sources are defined as NO_x recycled from HNO_3, PAN, or other NO_y species. For regions having very weak primary sources the latter source type can become the dominant one.

Figure 12 shows the distribution of NO_x for PEM-B (20-30°N) and PEM-A (18-42°N). Although this summary data indicate that at all altitudes NO_x mixing ratios for PEM-B exceeded those for PEM-A, the difference for altitudes above 4 km is quite modest, that is, typically a factor of 1.6 or less. For the lower troposphere the large NO_x difference has already been addressed in terms of the major influence from continental outflow. The chemical make-up of this outflow was dominated by anthropogenic emissions. As this continental air mass was advected out into the western Pacific at low altitudes, high levels of NO_x were maintained by the recycling of NO_x from PAN (~200 pptv). Model simulations suggest that as much as 50% of the observed NO_x for altitudes of 0-1 km and 20% at 1-2 km could have been derived from PAN. Above 2 km this source was found to be negligibly small.

For the upper free troposphere the relative amounts of different NO_x sources represent a far more complex issue. A more detailed analysis of high-altitude sources for both PEM-A and PEM-B is in progress and will be published independently (*D.D. Davis et al.*, unpublished results, 1997). Model calculations suggest that for PEM-B as much as 32% of the upper free tropospheric NO_x could be explained by the recycling of NO_x through HNO_3 (~120 pptv) with virtually no contribution coming from PAN (~60 pptv). The remaining high-altitude NO_x appears to be made up of a combination of primary sources. Chemical fingerprints identified in time series plots of the high-altitude data suggest that the primary sources include aircraft emissions, stratospheric intrusions, transport of surface emissions to high altitudes, and even some small contribution from lightning.

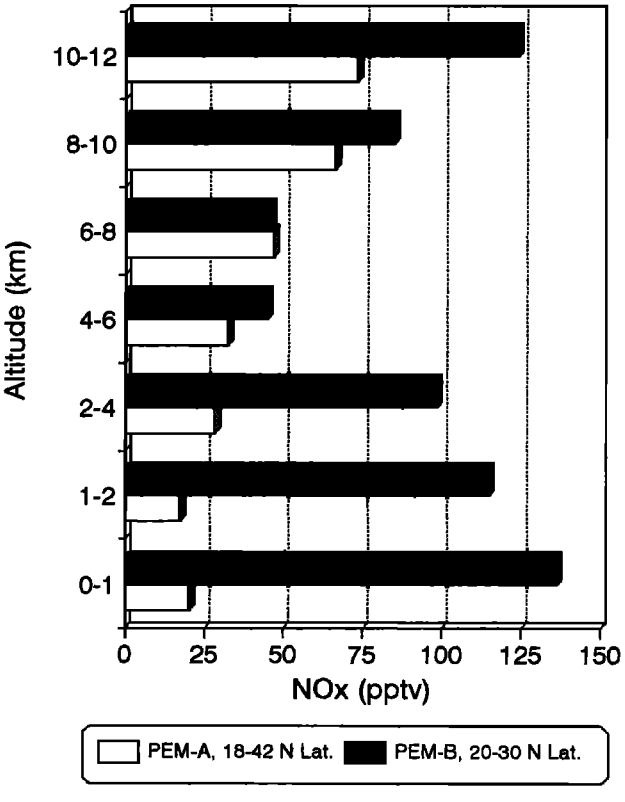

Figure 12. Median altitude distribution of NO_x for PEM-West A (18-42°N) and PEM-West B (20-30°N).

5. Summary and Conclusions

An analysis of O_3 photochemistry for the extratropical component of the PEM-B field program has revealed a region made up of two distinct photochemical regimes: 20-30°N and 30-50°N. Common to both regimes was the influence of continental outflow from the western Pacific Rim. In both cases the chemical nature of the outflow reflected anthropogenic emissions. A major difference between the two regimes was the tropopause height and the level of actinic flux resulting in highly elevated values of $J(O^1D)$ for 20-30°N relative to 30-50°N.

Diurnal-average O_3 formation rates for 20-30°N exceeded those for 30-50°N by factors of 3-13. For O_3 destruction the difference was even greater, involving factors of 4-14. In spite of these large differences, both regimes still exhibited net photochemical production of O_3 at all altitudes. This first of its kind observation for a large segment of the northwestern Pacific is quite unusual, both because the lower marine troposphere is typically a region found to exhibit net photochemical destruction and because the season of the year was late winter/early spring. As noted above, the low-altitude outflow of continental emissions was a critical factor in creating conditions in which net O_3 production prevailed for both regimes. This was apparent in the observed elevated levels of NO and CO as well as numerous NMHCs. It was also evident in the contribution to O_3 formation from organic peroxy radicals (RO_2) of 10-20% for altitudes less than 4 km.

Despite the much lower values for O_3 formation and destruction at 30-50°N, net O_3 production below 2 km was still estimated to be as large as that calculated at 20-30°N. This result strongly reflects the influence of having much lower values of NO_{crit} at 30-50°N than at 20-30°N. For example, even though NO levels in both regimes were in the 20-30 pptv range, 30-50°N had an excess of 20 pptv NO (above NO_{crit}), while for 20-30°N the excess was only 4 pptv.

For both latitude ranges a significant fraction of O_3 formation and destruction took place at altitudes below 4 km. The values were 67 and 81% for O_3 formation and 77 and 72% for O_3 destruction at 20-30°N and 30-50°N, respectively. The diurnal-average column-integrated rate of tropospheric O_3 formation for the 20-30°N regime exceeded the NH average stratospheric flux by an order of magnitude, while tropospheric column O_3 destruction exceeded surface deposition by a factor of 7. For 30-50°N the differences were much smaller, e.g., factors of 2 and 0.8, respectively.

Values for the tropospheric column-integrated O_3 tendency (e.g., 6.7×10^{10} and 21.4×10^{10} molecules/cm^2/s at 30-50°N and 20-30°N, respectively) suggest that the tropospheric O_3 column density was increasing at the rates of 1 and 2%/day. Although climatological data based on long term satellite observations would argue that for this season modest increases should occur, the increases estimated in this work are considerably greater than expected. Even so, it is unlikely that these rates could be sustained over any significant period of time due to springtime reductions in continental outflow as well as leveling effects driven by a linear dependence of $D(O_3)$ on ozone levels. In addition, one would expect a shortened lifetime for NO_x with increasing spring temperatures.

A comparison of the 20-30°N sampling regime of PEM-B with the comparable PEM-A latitude zone of 18-42°N has further demonstrated the impact of continental outflow during PEM-B. Most of this impact, however, was confined to altitudes below 4 km. For these altitudes, PEM-B ozone formation exceeded that for PEM-A by a factor of nearly 4. Integrated over all altitudes it was a factor of 2. Differences in ozone destruction were much smaller, amounting to only 15% overall, PEM-B being slightly higher.

A survey of both primary and secondary PEM-B NO_x sources indicated that below 4 km, continental outflow of anthropogenic emissions was clearly the dominant source; however, model simulations also suggest that recycling of NO_x from PAN could have contributed as much as 50% of the NO_x at altitudes below 1 km and as much as 20% between 1 and 2 km. For altitudes above 8 km, recycling of HNO_3 was estimated to account for one-third of the observed NO_x. In an independent study of the high-altitude PEM-B data, *D.D. Davis et al.* (unpublished results, 1997) have indicated that several primary NO_x sources contributed to the observed levels of NO_x including aircraft emissions, stratospheric intrusions, vertical transport of surface emissions, and a small contribution from lightning.

The results from this work are important in establishing that significant net production of O_3 can occur at extratropical latitudes even under wintertime conditions. Equally significant is the finding that these conditions can be found in a marine environment at low altitudes, an atmospheric domain typically dominated by net O_3 destruction. In the current study, outflow from the Asian continent maintained elevated levels of NO_x, CO, and NMHCs creating ideal conditions for O_3 production. While this impact is not totally unexpected in the near-coastal areas of a continent, this study has shown that outflow in some cases impacted on the western North Pacific at distances of 2000 km from the Asian Pacific Rim.

Acknowledgments. This work was supported in part by funds from the National Aeronautics and Space Administration under grants NCC-1-148 and 1438. D. D. Davis would also like to thank the project office at NASA Langley Research Center and the flight crews at NASA Ames Research Center for their dedicated support of the PEM-B program.

References

Chameides, W. L., and A. Tan, The two-dimensional diagnostic model for tropospheric OH: An uncertainty analysis, *J. Geophys. Res.*, *86*, 5209-5223, 1981.

Chameides, W. L., and J. C. G. Walker, A photochemical theory of tropospheric ozone, *J. Geophys. Res.*, *78*, 8751-8760, 1973.

Chameides, W. L., D. D. Davis, M. O. Rogers, J. Bradshaw, S. Sandholm, G. Sachse, G. Hill, G. Gregory, and R. Rasmussen, Net ozone photochemical production over the eastern and central North Pacific as inferred from GTE/CITE 1 observations during fall 1983, *J. Geophys. Res.*, *92*, 2131-2152, 1987.

Chatfield, R., and H. Harrison, Ozone in the remote troposphere: Mixing versus photochemistry, *J. Geophys. Res.*, *81*, 421-423, 1976.

Chen, G., A study of tropospheric photochemistry in the subtropical/tropical North and South Atlantic, Dissertation, 1995.

Crawford, J., et al., Photostationary state analysis of the NO_2-NO system based on airborne observations from the western and central North Pacific, *J. Geophys. Res.*, *101*, 2053-2072, 1996.

Crawford, J., et al., Implications of large-scale shifts in tropospheric NO_x levels in the remote tropical Pacific, *J. Geophys. Res.*, this issue.

Crutzen, P., A discussion of the chemistry of some minor constituents in the stratosphere and troposphere, *Pure Appl. Geophys.,106-108,* 1385-1399, 1973.

Davis, D. D., et al., A photostationary state analysis of the NO_2-NO system based on airborne observations from the subtropical/tropical North and South Atlantic, *J. Geophys. Res.*, *98*, 23,501-23,523, 1993.

Davis, D. D., et al., Assessment of the ozone photochemistry tendency in the western North Pacific as inferred from PEM-A observations during the fall of 1991, *J. Geophys. Res., 101*, 2111-2134, 1996.

Demore, W. B., S. P. Sander, D. M. Golden, R. F. Hampson, M. J. Kurylo, C. J. Howard, A. R. Ravishankara, C. E. Kolb, and M. J. Molina, Chemical kinetics and photochemical data for use in stratospheric modeling, *JPL Publ., 94-26*, 1994.

Fabian, P., Comments on "A photochemical theory of tropospheric ozone" by W. L. Chameides and J. C. G. Walker, *J. Geophys. Res., 79*, 4124-4125, 1974.

Fabian P., and P. G. Pruchniewicz, Meridional distribution of ozone in the troposphere and its seasonal variation, *J. Geophys. Res.*, *82*, 2063-2073, 1977.

Fishman, J., S. Solomon, and P. Crutzen, Observational and theoretical evidence in support of a significant in-situ photochemical source of tropospheric ozone, *Tellus*, *31*, 432-446, 1979.

Fishman, J., V. G. Brackett, and K. Fakhruzzaman, Distribution of tropospheric ozone in the tropics from satellite and ozonesonde measurements, *J. Atmos. Terr. Phys.*, *54*, 589-597, 1992.

Gidel, L. T., and M. A. Shapiro, General circulation model estimates of the net vertical flux of ozone in the lower stratosphere and the implications for the tropospheric ozone budget, *J. Geophys. Res.*, *85*, 4049-4058, 1980.

Hoell, J. M., D. D. Davis, S. C. Liu, R. Newell, M. Shipham, H. Akimoto, R. J. McNeal, R. J. Bendura, and J. W. Drewry, Pacific Exploratory Mission-West (PEM-A): September-October 1991, *J. Geophys. Res.*, *101*, 1641-1653, 1996.

Hoell, J. M., et al., Pacific Exploratory Mission-West (PEM-West B): February-March 1994, *J. Geophys. Res.*, this issue.

Hough, A. M., Development of a two-dimensional global tropospheric model: Model chemistry, *J. Geophys. Res.*, *96*, 7325-7362, 1991.

Hough, A. M., and R. G. Derwent, Changes in the global concentration of tropospheric ozone due to human activities, *Nature*, *344*, 645-650, 1990.

Isaksen, I. S. A., and Ø. Hov, Calculation of trends in the tropospheric concentration of O_3, OH, CO, CH_4, and NO_x, *Tellus Ser. B*, *39*, 271-285, 1987.

Jacob, D. J., et al., Origin of ozone and NO_x in the tropical troposphere: A photochemical analysis of aircraft observations over the South Atlantic basin, *J. Geophys. Res.*, *101*, 24,235-24,250, 1996.

Junkerman, W., U. Platt, and A. Volz-Thomas, A photoelectric detector for the measurement of photolysis frequencies of ozone and other atmospheric molecules, *J. Atmos. Chem.*, *8*, 203-227, 1989.

Kawa, S. R., and R. Pearson Jr., Ozone budgets from the dynamics and chemistry of marine stratocumulus experiment, *J. Geophys. Res.*, *94*, 9809-9817, 1989.

Lenschow, D. H., R. Pearson Jr., and B. B. Stankor, Measurements of ozone vertical flux to ocean and forest, *J. Geophys. Res.*, *87*, 8833-8837, 1982.

Liu, S. C., Possible effects on tropospheric O_3 and OH due to NO emissions, *Geophys. Res. Lett.*, *4*, 325-328, 1977.

Liu, S. C., D. Kley, M. McFarland, J. D. Mahlman, and H. Levy II, On the origin of tropospheric ozone, *J. Geophys. Res.*, *85*, 7546-7552, 1980.

Logan, J. A., Tropospheric ozone, seasonal behavior, trends, and anthropogenic influence, *J. Geophys. Res.*, *90*, 10,463-10,482, 1985.

Logan, J. A., M. J. Prather, S. C. Wofsy, and M. B. McElroy, Tropospheric chemistry: A global perspective, *J. Geophys. Res.*, *86*, 7210-7254, 1981.

Mahlman, J. D., H. Levy II, and W. J. Moxim, Three-dimensional tracer structure and behavior as simulated in two ozone precursor experiments, *J. Atmos. Sci.*, *37*, 655-685, 1980

Merrill, J. T., R. E. Newell, and A. S. Bachmeier, A meteorological overview for the Pacific Exploratory Mission-West, Phase B, *J. Geophys. Res.*, this issue.

Thompson, A. M., and R. W. Stewart, Effect of chemical kinetics uncertainties on calculated constituents in a tropospheric photochemical model, *J. Geophys. Res.*, *96*, 13,089-13,108, 1991.

Thompson, A. M., et al., Where did tropospheric ozone over southern Africa and the tropical Atlantic come from in October 1992? Insights from TOMS, GTE/TRACE A, and SAFARI 1992, *J. Geophys. Res.*, *101*, 24,251-24,278, 1996.

J. Crawford, D. Davis, G. Chen, S. Sandholm, and S. Liu, School of Earth and Atmospheric Sciences, Georgia Institute of Technology, 221 Bobby Dodd Way, Atlanta, GA 30332. (e-mail: douglas.davis@eas.gatech.edu; gc37@prism.gatech.edu; scott.sandholm@eas.gatech.edu; shaw.liu@eas.gatech.edu)

Y. Kondo, Solar Terrestrial Environmental Laboratory, Nagoya University, Toyokawa, Aichi, 442, Japan. (email: kondo@stelab.nagoya.u.ac.jp)

E. Browell, G. Gregory, B. Anderson, G. Sachse, J. Barrick, NASA Langley Research Center, Hampton, Virginia 23681. (e-mail: e.v.browell@larc.nasa.gov; g.l.gregory@larc.nasa.gov; b.e.anderson@larc.nasa.gov; g.w.sachse@larc.nasa.gov; j.d.barrick@larc.nasa.gov)

D. Blake, Chemistry CMOO-Gen Dept., CM-30, University of California, Irvine CA 92717. (e-mail: dblake@orion.oac.uci.edu)

R. Talbot, Institute for the Study of Earth, Oceans, and Space, Mores Hall, University of New Hampshire, Durham, NH 03824. (e-mail: rwt@christa.unh.edu)

H. Singh, NASA Ames Research Center, mail Stop 245-5, Moffett Field, California, 94035 (e-mail: hanwant_singh@qmgate.arc.nasa.gov)

(Received April 14, 1997; revised September 15, 1997; accepted September 15, 1997)